

Pressure dependent elastic, electronic, superconducting, and optical properties of ternary barium phosphides (BaM_2P_2 ; $M = \text{Ni, Rh}$): DFT based insights

Md. Maruf Mridha, S. H. Naqib*

Department of Physics, University of Rajshahi, Rajshahi 6205, Bangladesh

*Corresponding author: salehnaqib@yahoo.com

Abstract

Density functional theory (DFT) based first-principles investigations of structural, elastic, electronic band structure, and optical properties of superconducting ternary phosphides (BaM_2P_2 ; $M = \text{Ni, Rh}$) have been carried out in this study. This is the first detailed pressure dependent study of these properties for the titled compounds. The calculated ambient condition properties are compared with existing experimental and theoretical results, where available. The pressure dependent variations of the electronic density of states at the Fermi level, $N(E_F)$, and the Debye temperature, θ_D , have been studied and their effect on superconducting transition temperature have been explored. $N(E_F)$ shows nonmonotonic pressure dependence in BaNi_2P_2 . The pressure dependence of $N(E_F)$ for BaRh_2P_2 , on the other hand, is monotonic; decreasing with increasing pressure up to 15 GPa and saturating at higher pressure. Pressure dependence of $N(E_F)$ is reflected in the pressure dependent superconducting transition temperature. The Debye temperature increases with increasing pressure. The variation of the optical parameters (real and imaginary parts of the dielectric constant, refractive indices, reflectivity, absorption coefficient, and loss function) with photon energy show metallic behavior complementing the features of electronic band structure calculations. The absorption spectra of BaNi_2P_2 show strong optical absorption in the ultraviolet region, while BaRh_2P_2 absorbs photons over a wider energy band including the entire visible range. The reflectivity spectra for both BaNi_2P_2 and BaRh_2P_2 reveal that these materials are very strong reflectors of visible spectrum and particularly BaNi_2P_2 have significant potential to be used as coating material to reduce solar heating.

Keywords: Density functional theory (DFT); Ternary phosphide superconductors; Effect of pressure; Elastic constants; Electronic band structure; Optical properties

1 Introduction

The ternary low T_c phosphides, BaM_2P_2 ($M = \text{Ni, Rh}$), belong to the transition metal 122 compounds famous for exhibiting superconductivity over a wide range of critical temperatures and fascinating electronic ground states with varying degree of electronic correlations and

complexity [1]. The shorthand nomenclature ‘122’ originates from the stoichiometry of the materials. Compounds belonging to this group have a chemical formula AT_2Pn_2 , where A = alkaline-earth or rare-earth atom; T = transition metal atom; Pn = P, As, or Sb – one of the three pnictogens). The discovery of superconductivity with relatively high transition temperature in layered iron oxypnictide ($\text{La}[\text{O}_{1-x}\text{F}_x]\text{FeAs}$ with $x = 0.05 - 0.12$; $T_c = 26$ K) in early 2008 [2] induced a great deal of excitement within the condensed matter physics community [3]. Soon in the same year, superconductivity was found in a doped 122 compound ($\text{Ba}_{1-x}\text{K}_x\text{Fe}_2\text{As}_2$ [4] with a high T_c of 38 K. Since then, variety of 122 compounds has been discovered with different T_c s with and without Iron [1]. Not only that, superconductivity was also found in iron-free 122 phosphide and antimonide compounds [1, 5, 6]. Subsequently, it has been reported that these 122-compounds exhibit a number of intriguing electronic features, such as superconductivity [4], heavy fermion behavior [7], Kondo correlations [8], coexistence of superconductivity and magnetic orders and charge and spin density waves [1, 4, 7 – 10].

Quite generally, the 122 compounds with Fe show higher superconducting transition temperatures. At the same time, the role of magnetic order on superconductivity in these systems is still ambiguous [1]. Moreover, a number of studies on iron-based pnictides suggest that Fe atoms themselves carry no magnetic moment in these compounds [1], making the role of the transition metals in AT_2Pn_2 rather fascinating. 122 compounds assume ThCr_2Si_2 -type crystalline structure. Superconductivity is realized in doped $A\text{Fe}_2\text{As}_2$ on the A site (where $A = \text{Ba}, \text{Sr}, \text{Ca}, \text{Eu}$), under applied pressure in $A\text{Fe}_2\text{As}_2$, and at ambient pressure in the stoichiometric iron-free and iron-containing BaNi_2P_2 , LaRu_2P_2 , CsFe_2As_2 , and KFe_2As_2 metallic ternaries [11]. So far numerous studies have been done on the 122-type iron-based pnictides, to get further insight into the underlying physics of superconductivity in AT_2Pn_2 compounds, including the role of the transition metals and other novel properties. Many efforts on compounds without iron have also been made, both from experimental and theoretical aspects [1]. For compounds without Fe, LaRu_2P_2 , for example, superconducting transition takes place at 4.0 K [12]. Superconducting transition temperature for BaNi_2As_2 , on the other hand is 0.7 K [11]. This can be contrasted with the T_c of 38 K for isostructural $(\text{Ba}_{1-x}\text{K}_x)\text{Fe}_2\text{As}_2$. Understanding of all these diverse behaviors, as the rare-earth, transition metal and pnictogen atoms are varied, pose a serious challenge to the condensed matter physics community.

In this study we focus our attention on two low- T_c members of the 122 family, namely, BaNi_2P_2 ($T_c = 3.0$ K) [13] and BaRh_2P_2 ($T_c = 1.0$ K) [14, 15]. The role of these two elements on widely different values of superconducting transition temperatures of BaNi_2P_2 and BaRh_2P_2 is worth investigating. The structural features of BaNi_2P_2 have been known since the early experimental work by Keimeset al. [16]. Terashima et al. [17] have studied the de Haas van Alphen (dHvA) oscillation in BaNi_2P_2 . Ideta and co-workers [18], on the other hand, have reported the angle-resolved photoemission spectroscopy (ARPES) study of BaNi_2P_2 . Both these studies together revealed that the Fermi surface of this 122 compound has hole and electron sheets with three

strong dimensional features. A number of theoretical studies exist for BaNi_2P_2 . For example, electronic band structure of this compound was investigated by several groups [1, 19, 20]. All these band structure calculations reveal that the shallow valence electronic bands are constituted mainly from the Ni $3d$ orbitals with strong admixture with the P p electronic states.

In 2009, heat capacity, resistivity, and uniform magnetic susceptibility studies showed bulk superconductivity in BaIr_2P_2 ($T_c = 2.1$ K) and BaRh_2P_2 ($T_c = 1.0$ K) single crystals with ThCr_2Si_2 -type crystalline structure [14, 15]. These two compounds were known since the early work of Wurth et al. [21] and Lohken et al. [22], even though their superconducting state remained unexplored. These two compounds (and BaNi_2P_2) are isostructural to LaRu_2P_2 and altogether they amply illustrate the existence of superconductivity over a large variety of layered transition metal pnictides. The density functional theory (DFT) based investigation by Shein and Ivanovskii on ternary 122 phosphides [23] indicates that the electronic energy density of states at the Fermi level, $N(E_F)$, is markedly larger for BaRh_2P_2 in comparison with that for BaIr_2P_2 although the T_c of the former is very much lower than that of the later. This led Shein and Ivanovskii [23] suggest that the increase in T_c from 1.0 K for BaRh_2P_2 to 2.1 K for BaIr_2P_2 can be related to the difference in the phonon spectrum of these compounds. Existing experimental [14, 15, 24] and theoretical studies [24, 25] on 122 ternary phosphide superconductors imply that the strength of the interlayer P-P bonding plays a crucial part for superconductivity in these systems.

It is hard to overstate the role of pressure in understanding, modifying, and exploring the superconducting correlations in elements, compounds and solid solutions. It is the concept of chemical pressure that led to the discovery of Y123 ($\text{YBa}_2\text{Cu}_3\text{O}_x$; the first superconducting compound with a transition temperature above the boiling point of liquid nitrogen) high- T_c cuprate superconductor [26]. The pressure dependence of the superconducting transition temperature can yield a wealth of information regarding the structural, lattice dynamical, and electronic band structure related features (e.g., the electronic energy density of the states at the Fermi level) directly linked to the emergence of superconductivity [27 – 29]. To the best of our knowledge, pressure dependent ab-initio study on superconducting 122 ternary phosphides is scarce in the existing literature. This is one of the main motivations for this pressure dependent ab-initio study of BaNi_2P_2 and BaRh_2P_2 compounds. As far as we are aware of, there is no investigation on the optical properties of these two systems. From a number of recent investigations on layered ternaries belonging to different classes, we have found that these compounds often possess attractive optical features which are suitable for variety of optoelectronic device applications [30 – 36]. Therefore, we have undertaken this project also to investigate the energy dependent optical constants of BaNi_2P_2 and BaRh_2P_2 in detail. It is worth noting that energy dependent optical response of a material is intimately related to the underlying electronic band structure and provides one with information that complements the band structure calculations.

The rest of this paper has been organized as follows. Section 2 consists of a description of the theoretical formalism employed in calculations of the physical properties. In Section 3 we have presented and analyzed the results of calculations. Finally, in Section 4, the results are discussed and important conclusions are drawn.

2 Computational methodologies

It is fair to say that the most popular practical approach to *ab-initio* modeling of structural and electronic properties of crystalline solids is the DFT with periodic boundary conditions. In this approach the ground state of the compound is found by solving the Kohn-Sham equation [37]. The choice of exchange-correlations potential is quite important for the reliable estimates of the ground state physical properties of the system. For metallic systems with weak electronic correlations, the generalized gradient approximation (GGA) is often a good starting point keeping in the mind that GGA has a tendency of relaxing the crystal lattice and slightly overestimating the lattice constants. For solids with high electron density and a small deviation from the average, local density approximation (LDA) is prescribed. Unlike GGA, LDA contracts the lattice due to localized nature of the trial electronic orbitals [38]. In this study, in view of the known characteristics of BaM_2P_2 ($M = Ni, Rh$) [11, 13 – 16], we have used the GGA with the Perdew-Burke-Ernzerhof (PBE) functional [39] as contained within the CAMbridge Serial Total Energy Package (CASTEP) [40]. This particular functional is well known for its general applicability and gives rather accurate results for diverse class of crystalline solids. We have also used Vanderbilt-type ultra-soft pseudopotentials to take into account of the electron-ion interactions [41]. This particular pseudopotential relaxes the norm-conserving criteria but at the same time produces a smooth and computation friendly procedure to minimize the computational time without compromising the accuracy of the results appreciably. Broyden Fletcher Goldfarb Shanno (BFGS) geometry optimization [42] technique was used to optimize the crystal structure for the given symmetry ($I4/mmm$, space group No. 139). The following electronic states have been considered for the band structure calculations: Ba [$5p5d6s$], Ni [$3p3d4s$], Rh [$4p4d5s$], P [$3s3p$]. Periodic Bloch boundary conditions have been used to determine the total energies of the cell volume. Tolerance levels for computations were set such that very high level of convergence was achieved. An energy cut-off of 500 eV was used for the expansion of the plane wave basis set. k -point sampling within the first Brillouin zone (BZ) for the compounds under study was carried out following the Monkhorst-pack grid scheme [43]. For precise k -space integration, $15 \times 15 \times 7$ and $12 \times 12 \times 6$ k -point grids were used to sample the BZ for $BaNi_2P_2$ and $BaRh_2P_2$, respectively. The tolerance levels for computational convergence were set to ultra-fine. We have calculated the single crystal elastic constants by the ‘stress-strain’ method contained within the CASTEP code, where elastic responses of the optimized structure corresponding to various stress components are considered. The bulk modulus, B and the modulus of rigidity (shear modulus), G were calculated from the estimated single crystal elastic constants, C_{ij} . Elastic constants and moduli are linked to the average velocity of sound in a crystalline solid. This sound velocity, on the other hand depends on the Debye temperature. Utilizing this link, the Debye temperatures of

BaM₂P₂ have been calculated at different pressures. The electronic band structure has been investigated using the theoretically optimized geometry of BaM₂P₂. All the optical constants were obtained by considering both interband and intraband photon induced electronic transition probabilities. The imaginary part, $\varepsilon_2(\omega)$, of the complex dielectric function, $\varepsilon(\omega)$ ($= \varepsilon_1(\omega) + i\varepsilon_2(\omega)$) has been calculated from the matrix elements of electronic transition between occupied and unoccupied orbitals by employing the CASTEP supported formula given by-

$$\varepsilon_2(\omega) = \frac{2e^2\pi}{\Omega\varepsilon_0} \sum_{k,v,c} \left| \langle \psi_k^c | \hat{u} \cdot \vec{r} | \psi_k^v \rangle \right|^2 \delta(E_k^c - E_k^v - E) \quad (1)$$

In this equation, Ω is the volume of the unit cell, ω is the angular frequency of the incident electromagnetic wave (photon), e is the electronic charge, ψ_k^c and ψ_k^v are the conduction and valence band wave functions at a fixed wave-vector k . The delta function ensures conservation of energy and momentum during the optical transition. It should be mentioned that Eqn. 1 has been written for interband transitions. This equation is equally valid for intraband optical transitions with relevant changes in the energy level/band indices. The real part of the dielectric constant $\varepsilon_1(\omega)$ of the dielectric function can be extracted from the corresponding imaginary part $\varepsilon_2(\omega)$ via the Kramers-Kronig equations. Once these two parts of the energy dependent dielectric constant are known, all the other optical parameters can be evaluated from them [44]. This procedure has been used extensively by a volume of earlier studies to accurately calculate the frequency dependent optical constants for compounds belonging to diverse classes of materials with widely varying electronic band structures [30 – 36, 45].

3 Theoretical results

3.1 Structural and elastic properties

As mentioned earlier BaM₂P₂ compounds crystallize in ThCr₂Si₂-type structure belonging to the space group I4/*mmm* (body centered tetragonal). Fig. 1 shows the schematic crystal structure of BaM₂P₂. The optimized lattice constants and cell volumes under different uniform pressure are presented in Table 1. Ambient condition theoretical and experimental results from earlier studies [16, 20, 21, 23, 46, 47] are also given in this table, where available. It is seen that the optimized structural parameters under ambient condition agree well with prior results [16, 20, 21, 23, 46, 47]. In fact the zero-pressure values of the lattice parameters and cell volumes obtained here agree to a better extent with the experimental values compared to some of the other theoretical estimates [23, 46]. Due to the tetragonal structural symmetry the compounds under study possess six independent single crystal elastic constants (C_{ij}), designated by C_{11} , C_{33} , C_{44} , C_{66} , C_{12} , and C_{13} . We have tabulated the calculated C_{ij} for BaM₂P₂ at different pressures in Table 2 together with the existing theoretical estimates [47, 48]. A crystal with given symmetry is elastically or mechanically stable if the elastic energy corresponding to an arbitrary strain within

the elastic limit is positive. This requirement leads to the following four necessary and sufficient conditions for mechanical stability of tetragonal systems [49]:

$$C_{11} > |C_{12}|; 2C_{13}^2 < C_{33}(C_{11} + C_{12}); C_{44} > 0; C_{66} > 0$$

From the tabulated values of C_{ij} and the conditions for stability, it is evident that both BaNi_2P_2 and BaRh_2P_2 are mechanically stable. Among the six independent elastic constants, C_{11} ($= C_{22}$) and C_{33} measure the elastic response of the compound due to uniaxial stresses. C_{44} and C_{44} arise in reaction to shearing stresses. C_{12} and C_{13} , on the other hand measure the response due to an axial stress with respect to a strain along a perpendicular axis. The elastic moduli can be calculated from the calculated values of C_{ij} .

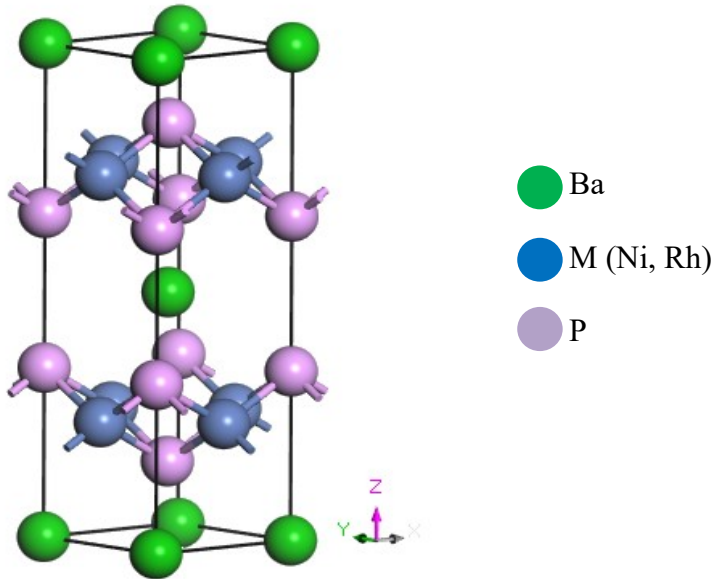


Figure 1: Schematic crystal structure of BaM_2P_2 . The crystallographic directions are shown.

Table 1: Optimized structural parameters of BaM_2P_2 at different pressures.

Pressure (GPa)	Compound	Lattice Parameter			Volume	Reference
		$a(\text{\AA})$	$b(\text{\AA})$	$c(\text{\AA})$	$V(\text{\AA}^3)$	
0	BaNi ₂ P ₂	3.941	3.941	12.008	186.532	This work
5		3.869	3.869	11.751	175.883	
10		3.806	3.806	11.573	167.661	
15		3.762	3.762	11.392	161.195	
20		3.724	3.724	11.236	155.815	
0		3.947	3.947	11.820	184.141	Expt. [16]
0		3.956	3.956	11.995	187.721	Theo. [23]
0		3.945	3.945	11.814	183.862	Theo. [20]
0		3.983	3.983	12.079	191.625	Theo. [46]
0	BaRh ₂ P ₂	4.001	4.001	12.619	202.05	This work
5		3.953	3.953	11.279	191.912	
10		3.915	3.915	11.984	183.737	
15		3.885	3.885	11.733	177.169	
20		3.862	3.862	11.488	171.412	
0		3.939	3.939	12.576	195.125	Expt. [21]
0		4.040	4.040	12.375	201.97	Theo. [47]

Table 2: Single crystal elastic constants (C_{ij} in GPa) of BaM_2P_2 at different pressures.

Pressure (GPa)	Compound	C_{11}	C_{33}	C_{44}	C_{66}	C_{12}	C_{13}	Refs.
0	BaNi ₂ P ₂	124.702	107.218	38.14	23.975	-21.29	27.96	This
5		161.658	113.81	51.62	32.953	7.14	60.743	This
10		220.55	140.88	65.576	39.13	59.723	112.363	This
15		228.461	184.239	78.459	44.091	62.686	116.329	This
20		222.052	124.660	89.318	48.744	54.954	108.578	This
0		171.91	89.25	43.84	23.04	21.23	66.51	Theo. [48]
0	BaRh ₂ P ₂	162.586	104.518	39.607	68.094	57.621	57.547	This
5		205.048	128.131	53.598	100.885	90.481	77.339	This
10		233.863	162.046	62.839	121.715	115.035	91.363	This
15		259.092	187.261	73.135	137.568	136.694	112.054	This
20		278.497	185.347	81.518	150.532	156.95	130.868	This
0		147.26	89.79	26.81	53.39	57.75	60.50	Theo. [47]

In [Table 2](#), it is interesting to note that at zero pressure C_{12} of BaNi_2P_2 shows a negative value. This is not entirely unusual. For example, compounds where atoms have mixed valency can show negative off-diagonal elastic constants together with mechanical stability [50]. In some cases, negative elastic constant implies existence of internal stress inside the compound. It is interesting to note that all the elastic constants are positive and increase with increasing pressure up to 15 GPa. At higher pressure (20 GPa), some of the elastic constants exhibit a decreasing trend. This may imply some tendency towards pressure induced structural instability in BaM_2P_2 . From [Table 2](#) it is seen that, $C_{11} > C_{33}$ at all pressures for both the compounds. The difference becomes more prominent as pressure increases. This indicates that the structure is stiffer along the [100] and [010] directions in comparison to that along the [001] direction, as far as the uniaxial stiffness is concerned. Such behavior is directly related to the strength of the chemical bonding in the respective crystallographic directions within the compound. [Table 2](#) also shows that $C_{44} > C_{66}$, at all pressures. The principle implication of this finding is that, the [100] (010) shear should be more effective in changing the shape than the [100] (001) shear for BaM_2As_2 compounds. All these qualitative and quantitative features of C_{ij} strongly reflect the layered features of the crystal structure under consideration. From the values of C_{ij} it becomes evident that chemical bondings within the ab -plane are stronger than those along c -direction.

As mentioned earlier, various elastic moduli, the Poisson's ratio and the Pugh's ratio can be estimated from the calculated single crystal elastic constants C_{ij} . [Table 3](#) shows these polycrystalline elastic moduli and ratios of BaM_2P_2 at different applied pressures. The Voigt approximation [51] asserts that isotropic bulk and shear moduli can be extracted from linear combinations of various single crystal elastic constants [51 – 54]. The Voigt approximated bulk and shear moduli have been denoted by B_V and G_V , respectively. Reuss, on the other hand, derived [55] different estimates for isotropic bulk and shear moduli from the single crystal elastic constants [52 – 54] using different criteria. Reuss approximated elastic moduli are denoted by B_R and G_R . Subsequently, Hill [56] proved that, the Voigt and Reuss approximated estimates are actually the upper and lower limits of the polycrystalline elastic moduli. A realistic measure of the bulk and shear moduli are therefore, the arithmetic averages given by, $B = (B_V + B_R)/2$ and $G = (G_V + G_R)/2$, respectively. Both Young's modulus, Y , and Poisson's ratio, n , are related to the bulk modulus and to the shear modulus [52 – 54]. The Pugh's ratio, expressed as B/G , is an important elastic indicator which is also presented in [Table 3](#).

Table 3: Polycrystalline bulk modulus B_V , B_R , B (in GPa), shear modulus G_V , G_R , G (in GPa), Young modulus Y (in GPa), Pugh's ratio B/G and Poisson's ratio n for BaM_2P_2 .

Pressure (GPa)	Compound	B_V	B_R	B	G_V	G_R	G	Y	B/G	n	Refs.
0	BaNi ₂ P ₂	47.32	46.23	46.77	41.52	36.32	38.92	91.41	1.20	0.17	This
5		77.15	77.11	77.13	47.81	41.27	44.54	112.05	1.72	0.26	This
10		127.87	126.43	127.15	53.89	40.85	47.37	126.42	2.70	0.33	This
15		136.87	136.77	136.82	63.26	54.86	59.06	154.89	2.32	0.31	This
20		123.67	119.04	121.35	65.25	40.78	53.01	138.83	2.32	0.31	This
0					80.92			35.87	93.87	2.27	0.30
0	BaRh ₂ P ₂	86.12	82.35	84.23	46.59	43.19	44.89	114.35	1.88	0.27	This
5		114.28	106.84	110.56	61.15	54.85	58.02	148.14	1.92	0.27	This
10		136.14	129.55	132.85	71.61	64.61	68.11	174.51	1.96	0.28	This
15		158.56	152.14	155.35	79.74	71.05	75.39	194.67	2.08	0.29	This
20		175.52	164.34	169.93	84.29	71.12	77.71	202.29	2.17	0.30	This
0			82.42	77.75	80.08	35.11	31.19	33.15	87.39	2.44	0.31

The pressure dependent variation of elastic moduli and ratios reveal several new interesting features of BaM_2P_2 . The bulk, shear and the Young moduli show conventional pressure dependence, namely, all these parameters increase with increasing pressure (except at 20 GPa for BaNi₂P₂). This is natural, since applied pressure makes the crystal stiffer. The intriguing part is in the pressure dependence of the Pugh's and Poisson's ratios.

For both the compounds under study, $B > G$, implying that they are prone to mechanical failure due to shearing deformation. Compared to many other metallic layered ternaries and their solid solutions, the elastic moduli of BaM_2P_2 are rather small [36, 57 – 61], indicating that these materials are relatively soft in nature. The ratio between polycrystalline bulk and shear moduli, known as the Pugh's ratio [62], is a useful indicator of mechanical behavior of solids. A large value of this ratio indicates ductile behavior; whereas a low value implies brittleness. The brittle to ductility boundary marked by a critical Pugh's ratio of 1.75. From Table 3 it is observed that applied pressure increases this ratio quite rapidly. For BaNi₂P₂, the Pugh's ratio at zero pressure is 1.20, implying ductility, at a pressure of 5 GPa this value increases to 1.72, close to the ductile to brittle boundary, for further increase in pressure, Pugh's ratio exceeds 1.75 and the compound is predicted to show highly brittle behavior. For BaRh₂P₂, the Pugh's ratio implies brittleness throughout but pressure increases its value systematically. Therefore, we conclude that the brittleness of BaRh₂P₂ increases with increasing applied pressure. Poisson's ratio is another significant measure that provides us with information not only about mechanical behavior but also about the underlying atomic bonding characteristics of a compound. It is known that $n = 0.25$ is the lower limit for solids where central-force field dominates [63]. The Poisson's ratio of BaNi₂P₂ shows strong pressure dependence. It rises sharply at low pressure. Poisson's ratio of

BaNi₂P₂ under ambient condition implies that non-central force dominates in electronic bondings in this compound, while the ratio at 5 GPa indicates the dominance of central forces in BaNi₂P₂. For BaRh₂P₂, the pressure dependence of n is significantly weaker. At all pressures including ambient the dominant bonding is central in nature. The brittle to ductile threshold is marked by a Poisson's ratio of ~ 0.31 [64]. This suggests that BaNi₂P₂ becomes brittle as pressure increases. The same pressure induced trend is observed for BaRh₂P₂. Relatively low values of Poisson's ratio for BaM₂P₂ indicate that atomic packing density is comparatively low in these compounds a characteristic of materials with substantial covalent and/or ionic bonding(s).

Measure of elastic anisotropy is a technologically important parameter. Elastic anisotropy influences variety of mechanical processes [65] such as the development of plastic deformations in crystals, propagation of cracks under external or nonequilibrium internal perturbations, microscale cracking in ceramics, alignment or misalignment of quantum dots, enhanced mobility of charged defects, plastic relaxation of thin films, etc. Hence, it is instructive to study the elastic anisotropy of compounds to understand their behavior under different conditions for possible engineering applications. Elastic anisotropy of crystalline solids is characterized by a number of anisotropy indices. Herein we have calculated a number of anisotropy factors of BaM₂P₂ in the body centered tetragonal form. The widely used anisotropic factors for tetragonal crystal structures are the three shear anisotropic factors, namely, A_1 , A_2 and A_3 . Furthermore, the anisotropy indices for the bulk and shear moduli, A_B and A_G , respectively, are also calculated. The universal anisotropic index, A_U , which applies to all crystal systems irrespective of the symmetry, has been computed. The relations connecting the anisotropy parameters to the elastic constants and moduli are given below [66, 67]:

$$A_1 = \frac{C_{44}(C_{11}+2C_{13}+C_{33})}{C_{11}C_{33}-C_{13}^2}, \text{ for the (010) or (100) plane.}$$

$$A_2 = \frac{C_{44}(C_L+2C_{13}+C_{33})}{C_L C_{33}-C_{13}^2}, \text{ for the (1}\bar{1}0\text{) plane, where } C_L = C_{66} + \frac{(C_{11}+C_{12})}{2}.$$

$$A_3 = \frac{2C_{66}}{C_{11}-C_{12}}, \text{ for the (001) plane.}$$

$$A_B = \frac{B_V-B_R}{B_V+B_R} \times 100; \quad A_G = \frac{G_V-G_R}{G_V+G_R} \times 100.$$

$$A_U = 5 \frac{G_V}{G_R} + \frac{B_V}{B_R} - 6.$$

All these anisotropy indices and their pressure dependences are displayed in [Table 4](#).

From physical ground, shear anisotropic factors determine the degree of anisotropies in the bonding strengths between atomic species located at different crystal planes. $A_i = 1$ ($i = 1, 2, 3$) suggests completely isotropic nature; deviation from unity suggests otherwise.

Table 4: Pressure dependent variation of elastic anisotropy factors of BaM_2P_2 .

Pressure (GPa)	Compound	A_1	A_2	A_3	A_B	A_G	A_U
0	BaNi ₂ P ₂	0.87	1.24	0.33	1.16	6.68	0.74
5		1.39	1.88	0.43	0.02	7.34	0.79
10		2.08	2.83	0.49	0.56	13.76	1.61
15		1.77	2.22	0.53	0.03	7.11	0.76
20		3.16	4.09	0.66	1.91	23.08	3.04
0	BaRh ₂ P ₂	1.10	1.02	1.29	2.24	3.78	0.44
5		1.28	1.10	1.76	3.36	5.43	0.64
10		1.23	1.01	2.05	2.48	5.14	0.59
15		1.36	1.09	2.25	2.06	5.76	0.65
20		1.71	1.29	2.48	3.29	8.47	0.99

The variations of anisotropy indices are quite interesting in the sense that these parameters show nonmonotonic pressure dependence for BaNi₂P₂. The anisotropy parameters increase steadily up to 10 GPa, decrease till 15 GPa and then increase sharply at 20 GPa. These are indicative of pressure dependent anisotropic change in the bonding characteristics and possible structural phase transition at high pressures. The behavior for BaRh₂P₂, on the other hand, is rather systematic. All the anisotropic indicators increase systematically except A_B . A_B of BaRh₂P₂ is nonmonotonic but the extent of variation is smaller than that for BaNi₂P₂.

The ratio between B and C_{44} can assess the machinability of a material via the machinability index, $\mu_M = B/C_{44}$ [68]. μ_M provides us with a value that designates the degree of ease with which a particular compound can be machined (cut or put into different shapes). A higher value corresponds to a better machinability. The pressure dependent μ_M of BaNi₂P₂ exhibits nonmonotonic behavior with the highest value of 1.94 at 10 GPa. μ_M of BaRh₂P₂ shows very weak dependence on applied pressure and lies between 2.06 to 2.12 at different pressures.

3.2 Debye temperature

As a fundamental lattice dynamical parameter Debye temperature, θ_D , correlates with many important thermo-physical properties of solids, such as heat capacity, bonding strengths, phonon thermal conductivity, vacancy formation energy, melting temperature etc. It also sets the characteristic energy scale which involves the electron-phonon coupling and Cooper pairing in superconductors. At low temperatures the vibrational excitations arise from acoustic modes. Hence, at low temperatures θ_D calculated from elastic constants is closely related to that determined from the heat capacity measurements. Among several methods for calculating θ_D , Anderson method is simple and straightforward, which depends on average sound velocity and can be expressed as [69]:

$$\theta_D = \frac{h}{k_B} \left[\left(\frac{3n}{4\pi} \right) \frac{N_A \rho}{M} \right]^{1/3} v_m \quad (2)$$

where h and k_B are the Planck's and Boltzmann's constants, respectively, N_A is the Avogadro's number, ρ denotes the mass density, M refers to the molecular weight and n is the number of atoms in a molecule. The sound wave, in a crystalline solid, has an average velocity v_m which can be determined from,

$$v_m = \left[\frac{1}{3} \left(\frac{1}{v_l^3} + \frac{2}{v_t^3} \right) \right]^{-1/3} \quad (3)$$

In Eqn. (3), v_l and v_t are the longitudinal and transverse sound velocities, respectively. These velocities can be determined using the following expressions [69]:

$$v_l = \left[\frac{3B + 4G}{3\rho} \right]^{1/2} \quad (4)$$

and

$$v_t = \left[\frac{G}{\rho} \right]^{1/2} \quad (5)$$

The estimated Debye temperature θ_D under different pressures along with the respective sound velocities v_l , v_t , and v_m for BaM_2P_2 compounds are enlisted in Table 5.

Table 5: The calculated crystal density ρ (gm/cm³), transverse (v_t), longitudinal (v_l), and average sound velocity v_m (m/s) and Debye temperature θ_D (K) of BaM_2P_2 at different pressures.

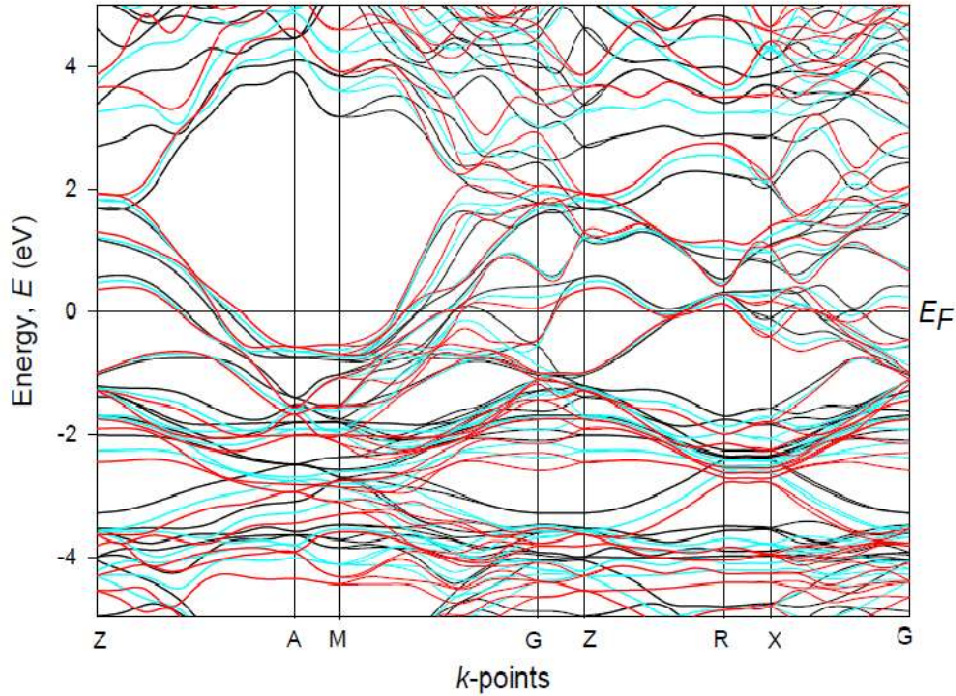
Pressure (GPa)	Compound	ρ	v_t	v_l	v_m	θ_D	Reference
0	BaNi ₂ P ₂	5.63	2629.25	4183.48	2681.73	301.10	This
5		5.97	2731.41	4779.35	2810.51	321.80	This
10		6.27	2748.64	5507.02	2855.17	332.17	This
15		6.52	3009.69	5747.89	3114.23	367.10	This
20		6.74	2804.45	5335.24	2903.17	346.11	This
0		-	-	-	-	290.00	Expt. [70]
0		5.68	2513.23	4761.23	2876.93	323.70	Theo. [47]
0	BaRh ₂ P ₂	6.65	2598.14	4652.32	2679.78	292.97	This
5		7.00	2878.98	5178.61	2967.45	330.03	This
10		7.32	3050.35	5524.86	3143.96	354.77	This
15		7.59	3151.63	5803.30	3251.31	371.37	This
20		7.84	3148.33	5904.04	3252.19	375.58	This
0			6.58	2244.54	4345.97	2512.93	273.91

Both Debye temperature and sound velocity increase systematically with pressure. This is mainly a consequence of pressure induced stiffening of the crystal. The agreements between previously determined θ_D and the present estimations are excellent [47, 48, 70].

3.3 Electronic band structure

Electronic band structure calculations are one of the most important features of crystalline solids which almost completely determine the charge transport and optical characteristics of materials. The band structure exhibits how the energy (E) of the allowed electronic states changes with the momentum ($\hbar k$) in the reciprocal lattice space. These $E(k)$ plots within the Brillouin zone are also known as the electronic dispersion curves. The electronic band structures at some selected pressures for BaM_2P_2 at different pressures are shown in Fig. 2.

(a)



(b)

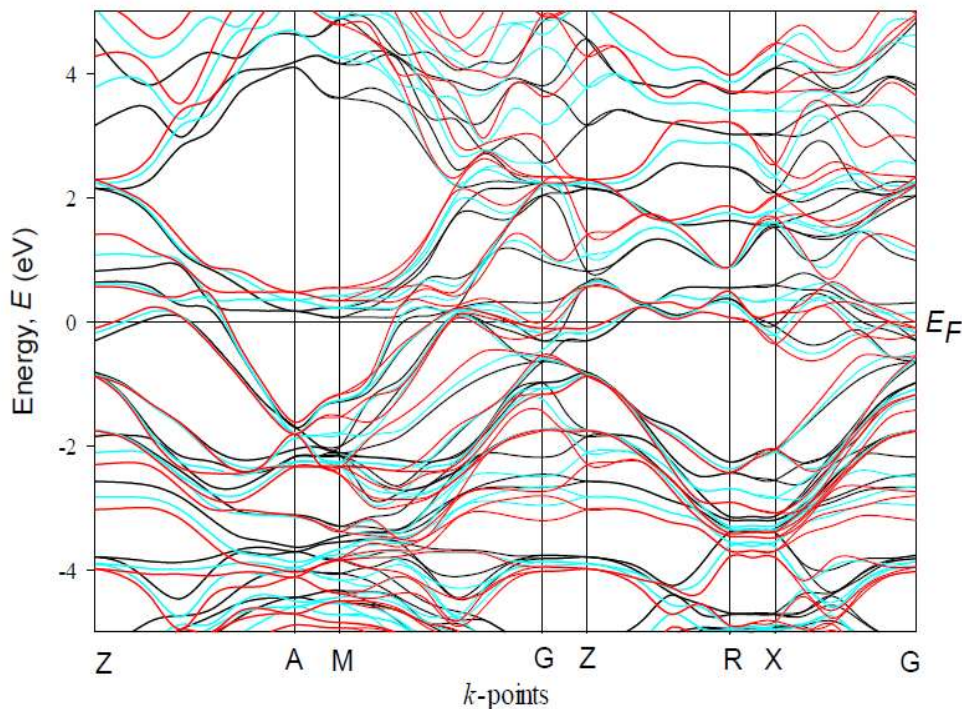


Figure 2: Electronic band structure of (a) BaNi₂P₂ and (b) BaRh₂P₂ at different representative pressures (black, cyan, and red lines are for pressures of 0, 10, 20 GPa, respectively). The Fermi level is marked by the horizontal line placed at 0 eV.

The band structures of BaM₂P₂ reveal clear metallic character as a number of bands cross the Fermi level (set at 0 eV) and there are significant valence and conduction band overlaps. The bands around E_F show dispersive features with varying degree. Among all these bands the ones running along $A - M$ show non-dispersive feature. This implies that effective mass of charge carriers are large in this direction and there is anisotropy in the charge transport. The band structure across the Fermi level also shows electron- and hole-like character. Therefore, the topography of the Fermi surface should contain both electron- and hole-sheets. Application of pressure has significant effect on the band structure. The pressure induced shift in the band structure is seen both below and above the Fermi energy. The energy shifts in the bands are mixed in character. Some of the bands show a decreasing trend in energy with increasing pressure; in some bands an opposite trend is seen. The degree of dispersion for the bands near the Fermi energy also varies with pressure. This implies that the transport properties of BaM₂P₂ will be affected significantly due to pressure. To explore the matter in greater depth, we have shown the orbital partial density of states (PDOS) and total density of states (TDOS) of BaM₂P₂ in Fig. 3 with different applied pressures.

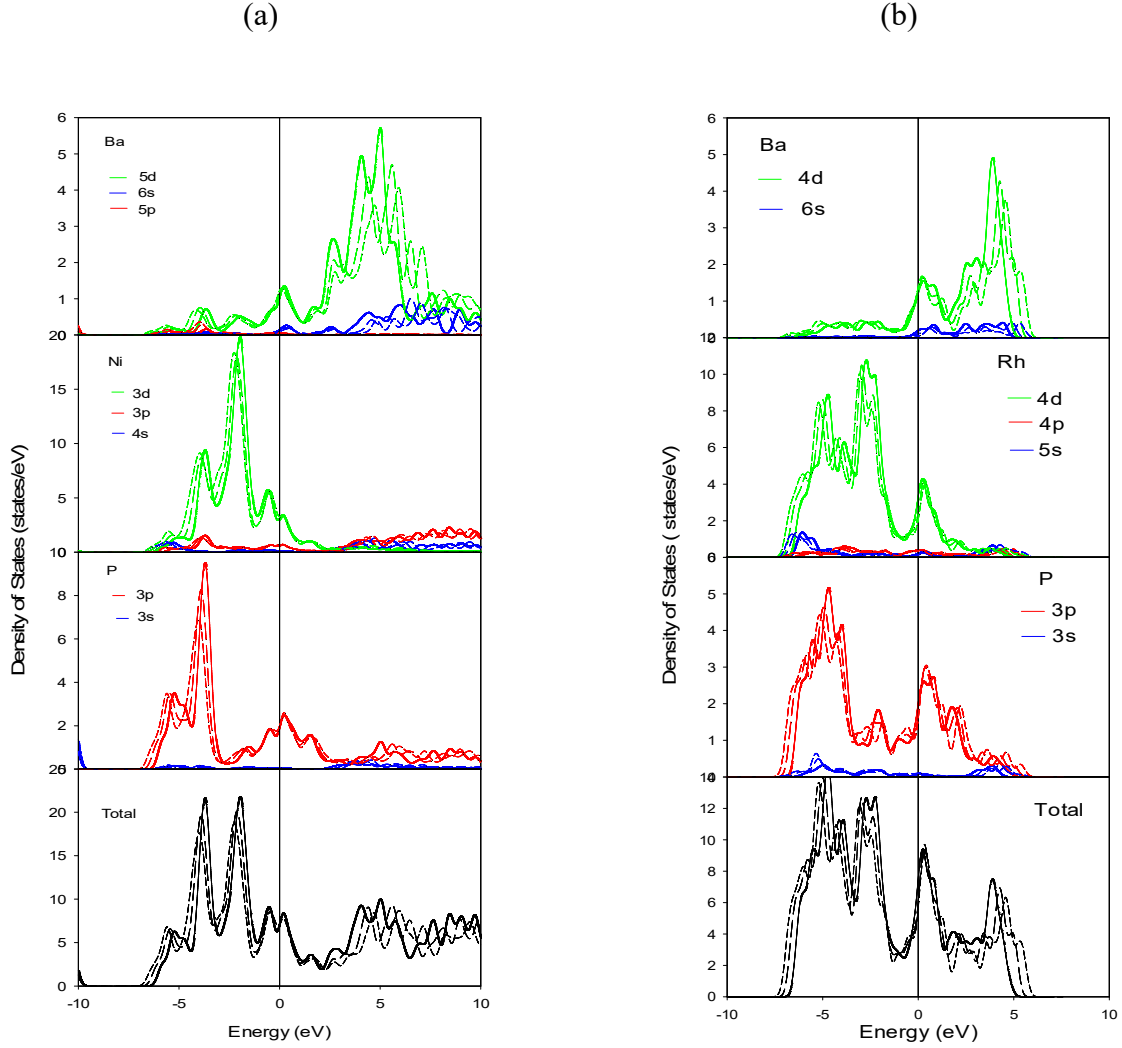


Figure 3: The PDOS and TDOS of (a) BaNi₂P₂ and (b) BaRh₂P₂ at different representative pressures (solid, short-dashed, and long-dashed lines are for pressures of 0, 5, 10 GPa, respectively).

Fig. 3a shows that the Ba 5*d*, Ni 3*d*, and P 3*p* states contribute significantly to the total electronic density of states at the Fermi level, $N(E_F)$ of BaNi₂P₂. Significant overlap in energy among these orbitals implies hybridization and tendency towards formation of covalent bondings. These three electronic states also contribute strongly in the formation of the valence band (VB) states below the Fermi level. Ba 6*s* and Ni 3*p* electronic states contribute in the conduction band (CB) above E_F . The main contributor for the conduction states is the Ba 5*d* orbital. In addition to several closely spaced peaks in the TDOS in the CB, there are two intense peaks in the VB centered on -2.0 eV and -4.0 eV. These two peaks are due to the Ni 3*d* and P 3*p* electronic states. These peaks are expected to play significant roles in determining the optical properties of BaNi₂P₂. The TDOS profile near the Fermi level is splitted for BaNi₂P₂. The Fermi level lies slightly towards

the antibonding (i.e., higher energy) peak. Finite value of $N(E_F)$ for BaNi_2P_2 confirms its metallic character.

Fig. 3b illustrates the PDOS and TDOS features of BaRh_2P_2 . It is seen that significant contribution to the $N(E_F)$ comes from the Ba $4d$, Rh $5s\ 4d$, and P $3p$ electronic states. There is large overlap among the PDOS due to Rh $5s\ 4d$ and P $3p$ orbitals around the Fermi energy. Therefore, the transport and bonding properties of BaRh_2P_2 are controlled by these electronic states and their hybridization. The TDOS at E_F for BaRh_2P_2 is comparable to that for BaNi_2P_2 . The Fermi level of BaRh_2P_2 lies quite close to a sharply rising peak in the TDOS little above E_F . This shows that electronic stability of BaRh_2P_2 is somewhat lower than that for BaNi_2P_2 . Two large peaks in the TDOS are found at around $-5\ \text{eV}$ and $-2.5\ \text{eV}$ in the VB. These peaks, together with the peak at $\sim 0.6\ \text{eV}$ in the CB are expected to contribute strongly to the matrix elements for optical transitions.

Pressure affects the band structure. It appears that pressure enlarges the bandwidths of VB and CB for both BaNi_2P_2 and BaRh_2P_2 . The TDOS at the Fermi level also changes with pressure. We discuss this pressure induced change in the TDOS and its implication on superconductivity in the next section.

3.4 Effect of pressure on superconductivity

BaM_2P_2 exhibits conventional phonon mediated superconductivity. Phase coherent Cooper pairs are formed and a symmetrical energy gap appears above and below the Fermi level at the superconducting transition temperature, T_c . For conventional superconductors Cooper pairs are formed due to attractive electron-phonon interaction. From weakly to moderately strongly coupled superconductors McMillan T_c -equation [71] can be employed to estimate T_c with high degree of accuracy. The expression for T_c is given below.

$$T_c = \frac{\theta_D}{1.45} \exp \left\{ -\frac{1.04(1 + \lambda)}{\lambda - \mu^*(1 + 0.62\lambda)} \right\} \quad (6)$$

In Eqn. (6), λ is the electron-phonon coupling constant and μ^* is the repulsive Coulomb pseudopotential. The electron-phonon coupling constant can be expressed as $\lambda = N(E_F)V_{\text{e-ph}}$, where $V_{\text{e-ph}}$ is the electron-phonon interaction energy responsible for Fermi surface instability and Cooper pairing [72]. One can calculate the pressure dependence of T_c by taking into account of the pressure dependent variation of θ_D and $N(E_F)$ BaM_2P_2 ($M = \text{Ni}, \text{Rh}$). These variations are shown in **Figs. 4**. First, we calculate the ambient pressure λ for BaM_2P_2 . The zero pressure electron-phonon coupling constants are found to be 0.60 and 0.45 for BaNi_2P_2 and BaRh_2P_2 , respectively. In our calculations, the value of Coulomb pseudopotential, μ^* has been taken as 0.13, a typical value for superconducting compounds [71]. Next, we have calculated $T_c(P)$ by using pressure dependent values of θ_D and $N(E_F)$, using Eqn. (6). The results of these calculations are depicted in **Fig. 5**. **Fig. 5** shows that T_c varies non-monotonically with pressure for BaNi_2P_2 , whereas for BaRh_2P_2 , T_c decreases with increasing pressure which flattens at high pressures.

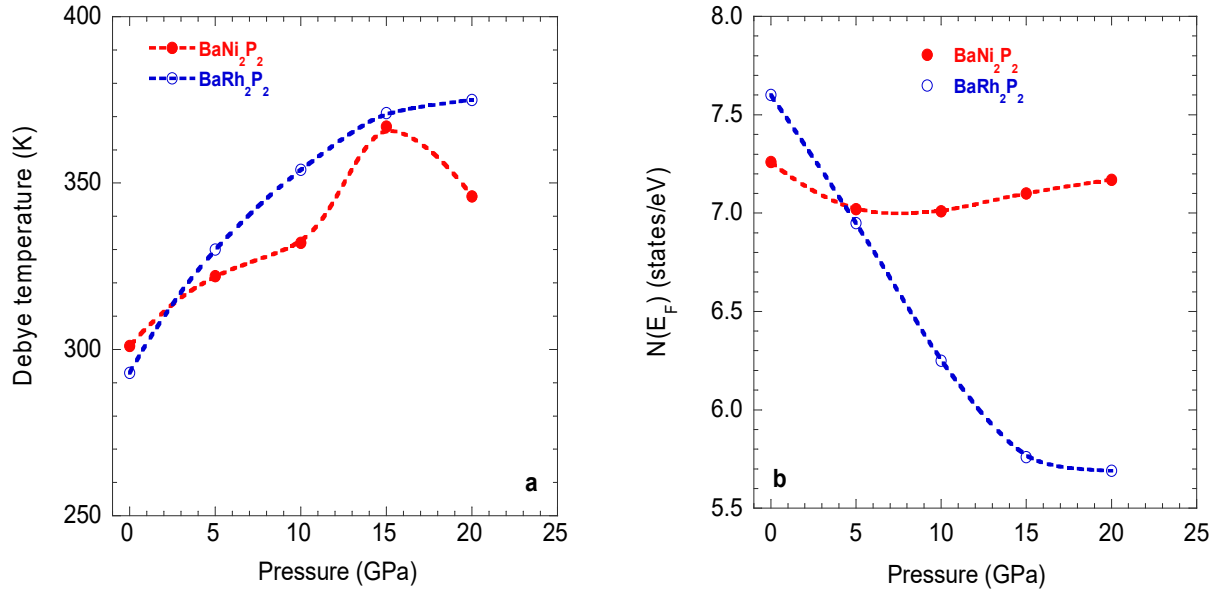


Figure 4: The pressure dependence of (a) θ_D and (b) $N(E_F)$ of BaNi₂P₂ and BaRh₂P₂.

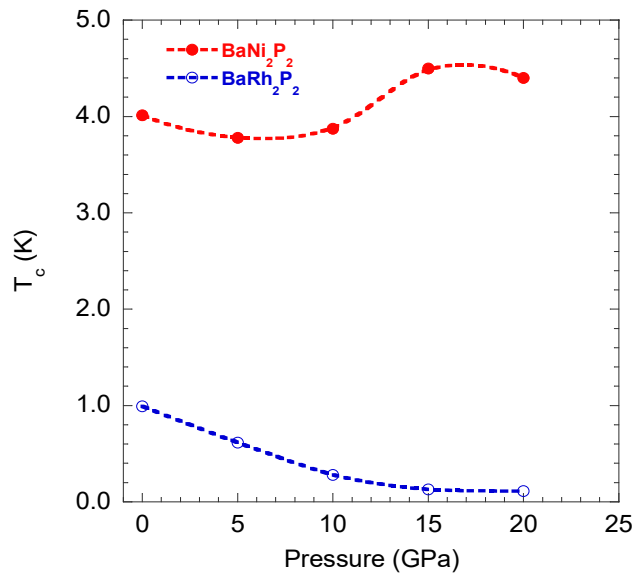


Figure 5: The pressure dependent superconducting transition temperatures of BaNi₂P₂ and BaRh₂P₂.

3.5 Optical properties of BaNi₂P₂ and BaRh₂P₂

Study of optical properties is important to understand the response of a material to incident electromagnetic wave. How various optical parameters behave at different spectral frequencies or energies are also important to explore possible optoelectronic and photovoltaic device applications of the compounds of interest. In this regard, the optical response of a compound to infrared, visible and ultraviolet spectra is particularly pertinent. A number of energy dependent (frequency) optical constants, namely real and imaginary part of dielectric constant $\epsilon_1(\omega)$ and $\epsilon_2(\omega)$, respectively, real part of refractive index $n(\omega)$, the extinction coefficient $k(\omega)$, energy loss function $L(\omega)$, real and imaginary parts of the optical conductivity ($\sigma_1(\omega)$ and $\sigma_2(\omega)$, respectively), reflectivity, $R(\omega)$, and the absorption coefficient $\alpha(\omega)$, are investigated to explore the response of BaM₂P₂ to incident photons with different energies. The energy dependent optical parameters are shown in Fig. 6.

The top panels of Fig. 6 exhibit the dielectric constants. The real part of the dielectric constant is related to the polarizability of the compound, the imaginary part, on the other hand gives a measure of the loss within the compound. $\epsilon_1(\omega)$ and $\epsilon_2(\omega)$ of BaM₂P₂ show clear metallic character, consistent with electronic band structure. The peak in the $\epsilon_1(\omega)$ and $\epsilon_2(\omega)$ of BaNi₂P₂ at ~ 8.0 eV arises from the optical transitions from the electronic states around -2.0 eV to -4.0 eV in the VB to the states around 5.0 eV in the CB (Fig. 3a, the TDOS plot). Similarly the weak peaks in the $\epsilon_1(\omega)$ and $\epsilon_2(\omega)$ of BaRh₂P₂ at ~ 7.5 eV originate from the electronic states around -6.0 eV in the VB to the states around 1.5 eV in the CB (Fig. 3b, the TDOS plot). The second pair of panels illustrates the complex refractive indices of BaNi₂P₂ and BaRh₂P₂. The real part of the refractive index determines the phase velocity of propagation the electromagnetic wave in the material. The imaginary part, often termed as the extinction coefficient, in contrast, measures the attenuation as the electromagnetic wave as it propagates through the compound. The real parts are quite high in the visible range of the optical spectra for both BaNi₂P₂ and BaRh₂P₂. The third pair of panels from the top shows the absorption spectra for BaNi₂P₂ and BaRh₂P₂. The optical absorption spectra of BaNi₂P₂ and BaRh₂P₂ are quite different although both show clear metallic character. The absorption coefficient for BaNi₂P₂ is significantly higher, characterized by prominent peaks at ~ 8.0 eV and ~ 18.0 eV in the ultraviolet region. Overall, BaNi₂P₂ absorbs ultraviolet (UV) radiation very effectively over an extended energy range from 7.0 eV to 20.0 eV. The absorption capability of BaRh₂P₂ is relatively low. A prominent peak in the absorption coefficient is located ~ 10.0 eV in the mid-UV region. The fourth pair of panels in Fig. 6 shows the reflectivity spectra of the compounds under consideration. BaNi₂P₂ has very interesting reflectivity characteristics. The reflectivity is very high, above 90% for the visible photons. The spectra also exhibit two distinct peaks. The first one is broad and the reflectivity remains above 80% in the energy range from 10.0 eV to 20.0 eV in the mid-UV region. The second peak is much sharper at resides around ~ 23.0 eV is the in the high energy region of the UV. The reflectivity of BaRh₂P₂ is significantly lower. This spectra show a peak around ~ 10.0 eV where

the reflectivity approaches almost 70%. The next pair of panels shows the optical conductivities. Optical conductivity once again confirms the metallic nature of the compounds.

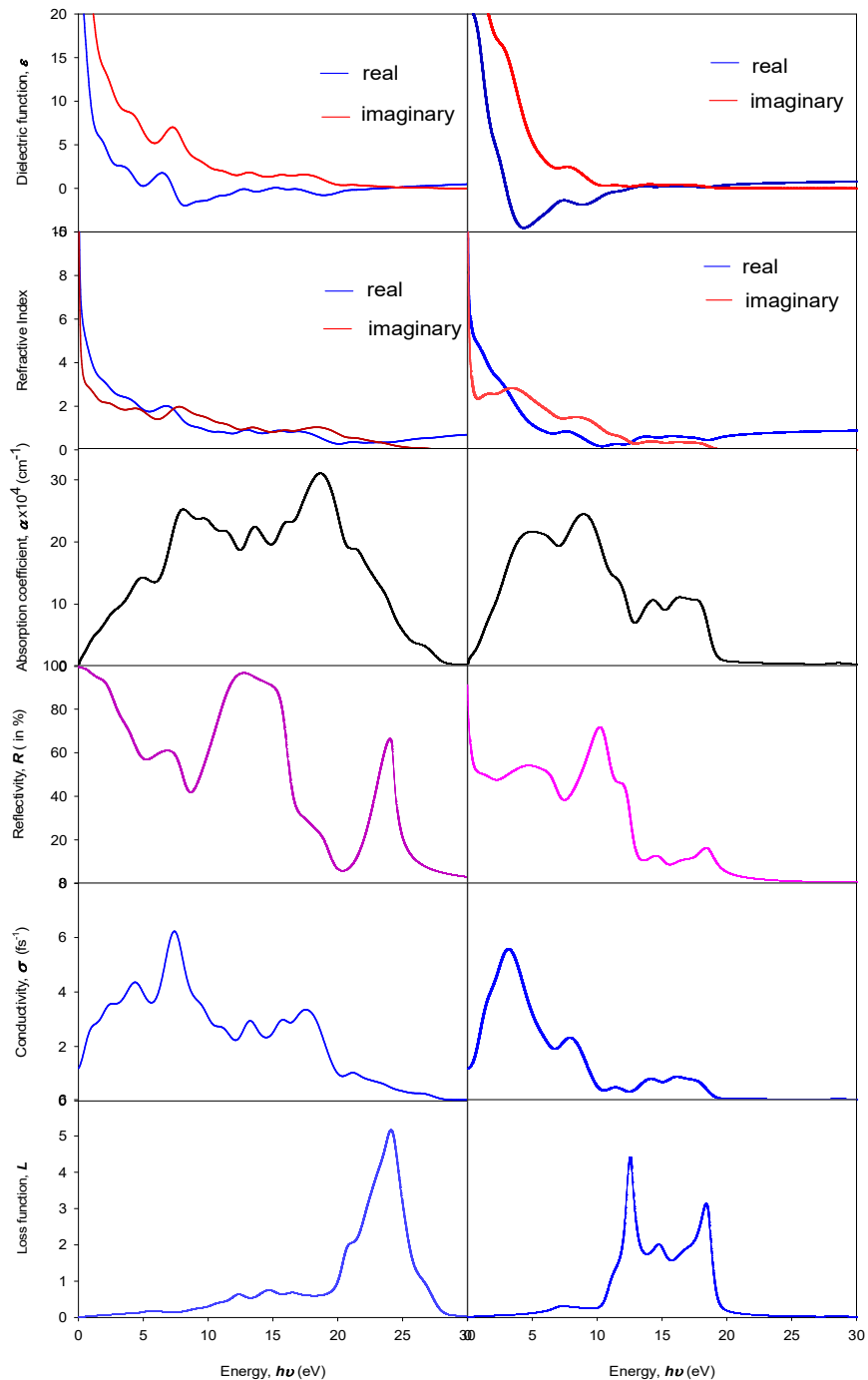


Figure 6: Dielectric constants, refractive indices, absorption coefficients, reflectivities, optical conductivities, and loss functions of BaNi₂P₂ and BaRh₂P₂ compounds.

Optical conductivity of BaNi_2P_2 is significantly higher than that of BaRh_2P_2 . The last (bottom) pair of panels of Fig. 6 shows the loss function of BaNi_2P_2 and BaRh_2P_2 . This particular optical parameter shows how a fast charged particle loss its energy via exciting plasmon modes as it passes through the compound. We see a strong plasma peak at ~ 24.0 eV for BaNi_2P_2 . For BaRh_2P_2 , multiple plasma peaks are observed. Peaks at ~ 12.5 eV and ~ 19.0 eV are prominent. It is interesting to know that at the plasma frequency, absorption, reflectivity and optical conductivity fall sharply. Above the plasma frequency, the compounds under consideration become transparent and show insulating character.

4 Discussion and conclusions

Detailed analyses of pressure dependent structural and elastic properties of BaNi_2P_2 and BaRh_2P_2 in the ThCr_2Si_2 -type body centered tetragonal structure have been performed. The pressure dependent single crystal elastic constants ensure mechanical stability up to 20 GPa (the upper limit of the pressure considered). Both BaNi_2P_2 and BaRh_2P_2 possess significant elastic anisotropy. Various anisotropy indices vary non-monotonically with pressure indicating the anisotropic nature in the atomic bonding strengths and layered nature of BaM_2P_2 ($M = \text{Ni}, \text{Rh}$). BaNi_2P_2 shows pressure induced ductile to brittle transition. BaRh_2P_2 , on the other hand remains brittle for pressures up to 20 GPa. The Poisson's ratios of BaM_2P_2 imply low packing density and mixed bonding character, dominated by covalent and ionic contributions. The machinability indices of the compounds under study at different pressures are quite high; comparable to those of many MAX phase nanolaminates [73]. BaRh_2P_2 is more machinable compared to BaNi_2P_2 . The Debye temperature, an important thermo-physical parameter of solids, was calculated from the elastic constants and crystal density. This particular method for calculating the Debye temperature from the elastic constants has been used extensively to reliably estimate θ_D for variety of compounds with different electronic ground states [57, 73 – 76]. θ_D is almost identical for both BaNi_2P_2 and BaRh_2P_2 , and shows conventional increasing trend with increasing pressure.

The electronic band structures and the PDOS and TDOS features of BaNi_2P_2 and BaRh_2P_2 are investigated in detail. The electronic band widths increase with increasing pressure. This is due to increase in the orbital overlap at increased pressure. The TDOS at the Fermi level for BaNi_2P_2 vary weakly with change in pressure but for BaRh_2P_2 , $N(E_F)$ decreases sharply with increasing pressure up to 15 GPa. Above this pressure, the variation flattens. We have calculated the pressure dependent superconducting transition temperature of BaNi_2P_2 and BaRh_2P_2 . Variation of the electron-phonon coupling constant with pressure has been estimated. T_c of BaNi_2P_2 varies non-monotonically with pressure. The overall variation is small. For BaRh_2P_2 , T_c decreases steadily with increasing pressure. This decrement is largely due to the reduction in the $N(E_F)$ with increasing pressure. The ambient pressure electron-phonon coupling constants for BaNi_2P_2 and BaRh_2P_2 are quite close to those for other isostructural APd_2As_2 ($A = \text{Ba}, \text{Sr}, \text{Ca}$) ternaries [74, 77]. Since $N(E_F)$ of BaNi_2P_2 and BaRh_2P_2 are comparable at zero pressure, the larger value

of λ of BaNi_2P_2 implies that the matrix element of the electron-phonon interaction energy is higher in this compound.

The energy dependent optical parameters confirm the metallic character of the compounds under study and are consistent with the electronic band structure, TDOS, and PDOS features. It is found that BaNi_2P_2 absorbs UV photons very effectively over an extended spectral range from 7.0 eV to 20.0 eV. This compound also reflects the visible radiations very effectively. Therefore, BaNi_2P_2 can be used as an efficient absorber of UV radiation and also as a reflecting coating material to reduce solar heating.

To summarize, we have investigated pressure dependent elastic, electronic, and superconducting properties of BaNi_2P_2 and BaRh_2P_2 via DFT based calculations. The optical properties at ambient pressure have also been investigated. The compounds under study, particularly BaNi_2P_2 , have attractive optical features suitable for possible applications.

Acknowledgements

S. H. N. acknowledges the research grant (1151/5/52/RU/Science-07/19-20) from the Faculty of Science, University of Rajshahi, Bangladesh, which partly supported this work. M. M. M. acknowledges the help from Professor F. Parvin, Department of Physics, University of Rajshahi, Bangladesh, for her help with the CASTEP program.

Data availability

The data sets generated and/or analyzed in this study are available from the corresponding author on reasonable request.

References

1. P. Zhang, Hui-fei Zhai, *Condens. Matter* 2(3) (2017) 28.
2. Y. Kamihara, T. Watanabe, M. Hirano, H. Hosono, *J. Am. Chem. Soc.* 130 (2008) 3296.
3. Qimiao Si, Rong Yu, Elihu Abrahams, *Nature Reviews Materials* 1 (2016) 16017.
4. M. Rotter, M. Tegel, D. Johrendt, *Phys. Rev. Lett.* 101 (2008) 107006.
5. F. Ronning, E. D. Bauer, T. Park, S. H. Baek, H. Sakai, J. D. Thompson, *Phys. Rev. B* 79 (2009) 134507.
6. M. Imai, S. Ibuka, N. Kikugawa, T. Terashima, S. Uji, T. Yajima, H. Kageyama, I. Hase, *Phys. Rev. B* 91 (2015) 014513.
7. Y. Hiranaka et al., *J. Phys. Soc. Jpn.* 82 (2013) 083708.
8. C. M. Feng et al., *Phys. Rev. B* 82 (2010) 094426.
9. Z. Ren, Q. Tao, S. Jiang, C. Feng, C. Wang, J. Dai, G. Cao, Z. Xu, *Phys. Rev. Lett.* 102 (2009) 137002.

10. K. Kudo, Y. Nishikubo, M. Nohara, *J. Phys. Soc. Jpn.* 79 (2010) 123710.
11. F. Ronning, N. Kurita, E. D. Bauer, B. L. Scott, T. Park, T. Klimczuk, R. Movshovich, J. D. Thompson, *J. Phys.: Condens. Matter* 20 (2008) 342203.
12. W. Jeitschko, R. Glaum, L. Boonk, *Solid State Chem.* 69 (1987)93.
13. T. Mine, H. Yanagi, T. Kamiya, Y. Kamihara, M. Hirano, H. Hosono, *Solid State Commun.* 147 (2008) 111.
14. N. Berry, C. Capan, G. Seyfarth, A. D. Bianchi, J. Ziller, Z. Fisk, *Phys. Rev. B* 79 (2009) 180502(R).
15. D. Hirai, T. Takayama, R. Higashinaka, H. Aruga-Katori, H. J. Takagi, *J. Phys. Soc. Jpn.* 78 (2009) 023706.
16. V. Keimes, D. Johrendt, A. Mewis, C. Hujnt, W. Schlabitz, *Z. Anorg. Allg. Chem.* 623 (1997) 1699.
17. T. Terashima, M. Kimata, H. Satsukawa, A. Harada, K. Hazama, M. Imai, S. Uji, H. Kito, A. Iyo, H. Eisaki, H. Harima, *J. Phys. Soc. Jpn.* 78 (2009) 033706.
18. S. Ideta et al., *Phys. Rev. B* 89(2014) 195138.
19. D. S. Jayalakshmi, M. Sundareswari, *Indian J. Phys.* 89 (2015) 201.
20. I. B. Shameem Banu, M. Rajagopalan, Mohammed Yousuf, P. Shenbagaraman, *J. Alloys Compd.* 288 (1999) 88.
21. A. Wurth, D. Johrendt, A. Mewis, C. Huhnt, G. Michels, M. Roepke, W. Z. Schlabitz, *Anorg. Allg. Chem.* 623 (1997) 1418.
22. A. Lohken, C. Lux, D. Johrendt, A. Z. Mewis, *Anorg. Allg. Chem.* 628 (2002) 1472.
23. I. R. Shein, A. L. Ivanovskii, *Phys. Rev. B* 79 (2009) 054510.
24. E. Razzoli et al., *Phys. Rev. Lett.* 108 (2012) 257005.
25. I. R. Shein, A. L. Ivanovskii, *JETP Lett.* 89(2009) 357.
26. M. K. Wu, J. R. Ashburn, C. J. Torng, P. H. Hor, R. L. Meng, L. Gao, Z. J. Huang, Y. Q. Wang, C. W. Chu, *Phys. Rev. Lett.* 58 (1987) 908.
27. Ayako Yamamoto, Nao Takeshita, Chieko Terakura, Yoshinori Tokura, *Nature Communications* 6 (2015) 8990.
28. C. Muryama, Y. Iye, T. Enomoto, N. Mori, Y. Yamada, T. Matsumoto, Y. Kobo, Y. Shimakawa, T. Manako, *Physica C* 183 (1991) 277.
29. R. S. Islam, S. H. Naqib, A. Islam, *J. Supercond.* 13 (2000) 485.
30. B. Rahman Rano, Istiaque M. Syed, S. H. Naqib, *J. Alloys Compd.* 829 (2020) 154522.
31. M. I. Naher, S. H. Naqib, *J. Alloys Compd.* 829 (2020) 154509.
32. Fazle Subhan et al., *J. Alloys Compd.* 785 (2019) 232.
33. Sikander Azam et al., *Physica B* (2020). <https://doi.org/10.1016/j.physb.2020.412056>
34. Sikander Azam et al., *Molecular Physics* (2019). <https://doi.org/10.1080/00268976.2019.1587026>
35. M. A. Ali et al., *J. Alloys Compd.* 781 (2019) 37.
36. F. Parvin, S. H. Naqib, *Chin. Phys. B* 26 (2017) 106201.

37. W. Kohn, L.J. Sham, Phys. Rev. 140 (1965) A1133–A1138.
<https://doi.org/10.1103/PhysRev.140.A1133>
38. M. M. Hossain, S.H. Naqib, Molecular Physics (2019).
<https://doi.org/10.1080/00268976.2019.1609706>
39. J. P. Perdew, K. Burke, M. Ernzerhof, Phys. Rev. Lett. 77 (1996) 3865.
40. S. J. Clark, M. D. Segall, C. J. Pickard, P. J. Hasnip, M. I. J. Probert, K. Refson, M. C. Payne, Zeitschrift Fur Krist. 220 (2005) 567.
<https://doi.org/10.1524/zkri.220.5.567.65075>
41. D. Vanderbilt, Phys. Rev. B 41 (1990) 7892.
42. T. H. Fischer, J. Almlöf, J. Phys. Chem. 96 (1992) 9768.
43. H. J. Monkhorst, J. D. Pack, Phys. Rev. B 13 (1976) 5188.
44. A. Chowdhury, M. A. Ali, M. M. Hossain, M. M. Uddin, S. H. Naqib, A. K. M. A. Islam Physica Status Solidi: B (2017) DOI: 10.1002/pssb.201700235
45. M. A. Ali, M. T. Nasir, M. R. Khatun, A. K. M. A. Islam, S. H. Naqib, Chinese Physics B 25 (2016) 103100.
46. Ertuğrul Karaca, H. M. Tütüncü, G. P. Srivastava, S. Uğur, Phys. Rev. B 94 (2016) 054507.
47. M. I. Kholil, M. S. Ali, M. Aftabuzzaman, J. Alloys Compd. 740(2018) 754.
48. Md. Atikur Rahman, Md. Zahidur Rahaman, Md. Lokman Ali, Md. Shahjahan Ali. arXiv:1801.10573 (2018).
49. Felix Mouhat, Francois-Xavier Coudert, Phys. Rev. B 90 (2014) 224104.
50. U. Scharer, P. Wachter, Solid State Communications 96 (1995) 497.
51. W. Voigt, Lehrbuch der Kristallphysik, Teubner, Leipzig, 1928.
52. M. A. Hadi, S. H. Naqib, S. R. G. Christopoulos, A. Chroneos, A. K. M. A. Islam, Journal of Alloys and Compounds 724 (2017) 1167.
53. M. A. Ali, M. M. Hossain, M. A. Hossain, M. T. Nasir, M. M. Uddin, M. Z. Hasan, A. K. M. A. Islam, S. H. Naqib, Journal of Alloys and Compounds 743 (2018) 146.
54. M. A. Hadi, M. Roknuzzaman, A. Chroneos, S. H. Naqib, A. K. M. A. Islam, R. V. Vovk, K. Ostrikov, Comp. Mater. Sci.137 (2017) 318.
55. A. Reuss, Berechnung der Fließgrenze von Mischkristallen auf Grund der Plastizitäts bedingung für Einkristalle, Z. Angew. Math. Mech. 9 (1929) 49-58.
56. R. Hill, J. Mech. Phys. Solids 11 (1963) 357.
57. M. A. Ali, M. A. Hadi, M. M. Hossain, S. H. Naqib, A. K. M. A. Islam, Phys. Status Solidi B. 254 (2017) 1700010.
58. M. Roknuzzaman, M. A. Hadi, M. J. Abden, M. T. Nasir, A. K. M. A. Islam, M. S. Ali, K. Ostrikov, S. H. Naqib, Comp. Mater. Sci.113 (2016)148.
59. M. A. Hadi, M. S. Ali, S. H. Naqib, A. K. M. A. Islam, Int. J. Comput. Mater. Sci. Eng. 2 (2013) 1350007.
60. P. Barua, M. M. Hossain, M. A. Ali, M. M. Uddin, S. H. Naqib, A. K. M. A. Islam, J. Alloy. Compd.770 (2019) 523.

61. F. Sultana, M. M. Uddin, M. A. Ali, M. M. Hossain, S. H. Naqib, A. K. M. A. Islam, *Results in Phys.* 11 (2018) 869.
62. S. F. Pugh, *Philos. Mag.* 45 (1954) 823.
63. M. H. Ledbetter, in *Materials at Low Temperatures*, edited by R. P. Reed and A. F. Clark (American Society for Metals, 1983).
64. G. N. Greaves, A. L. Greer, R. S. Lakes, T. Rouxel, *Nat. Mater.* 10 (2011) 823 and references therein.
65. C. M. Kube, *AIP Adv.* 6 (2016) 095209.
66. M-X. Zeng, R-N. Wang, B-Y. Tang, L-M. Peng, W-J. Ding, *Modelling Simul. Mater. Sci. Eng.* 20 (2012) 035018.
67. Z-J. Liu, S-Q. Duan, J. Yan, X-W. Sun, C-R. Zhang, Y-D. Chu, *Solid State Commun.* 150 (2010) 943.
68. Z. Sun, D. Music, R. Ahuja, J. M. Schneider, *Phys. Rev. B.* 71 (2005) 193402.
69. O. L. Anderson, H. H. Demarest Jr., *J. Geophys. Res.* 76 (1971) 1349.
70. D. Hirai, F. V. Rohr, R. J. Cava, *Phys. Rev. B* 86 (2012) 100505.
71. W. L. McMillan, *Phys. Rev.* 167 (1968) 331.
72. A. K. M. A. Islam, S. H. Naqib, *J. Phys. Chem. Solids* 58 (1997) 1153.
73. M. A. Hadi, N. Kelaidis, S. H. Naqib, A. Chroneos, A. K. M. A. Islam, *J. Phys. Chem. Solids* 129 (2019) 162.
74. F. Parvin, S. H. Naqib, *J. Alloy. Compd.* 780 (2019) 452.
75. M. A. Hadi, M. A. Alam, M. Roknuzzaman, M. T. Nasir, A. K. M. A. Islam, S. H. Naqib, *Chinese Phys. B.* 24 (2015) 117401.
76. M. A. Alam, M. A. Hadi, M. T. Nasir, M. Roknuzzaman, F. Parvin, M. K. Zilani, A. K. M. A. Islam, S. H. Naqib, *J. Supercond. Nov. Magn.* 29 (2016) 2503.
77. M. Abdel-Hafiez et al., *Phys. Rev. B* 97 (2018) 134508.

Author Contributions

S. H. N. designed the project and wrote the manuscript. M. M. M. performed the theoretical calculations and contributed in analysis. Both the authors reviewed the manuscript.

Additional Information

Competing Interests

The authors declare no competing interests.